



HAL
open science

Preparation and characterization of hollow silica nanocomposite functionalized with UV absorbable molybdenum cluster

Thi Kim Ngan Nguyen, Fabien Grasset, Stéphane Cordier, Maria Amela-Cortes, Yoshio Matsui, Naoki Ohashi, Naoto Shirahata, Tetsuo Uchikoshi

► To cite this version:

Thi Kim Ngan Nguyen, Fabien Grasset, Stéphane Cordier, Maria Amela-Cortes, Yoshio Matsui, et al.. Preparation and characterization of hollow silica nanocomposite functionalized with UV absorbable molybdenum cluster. *Advanced Powder Technology*, 2020, 31 (2), pp.895-903. 10.1016/j.appt.2019.12.009 . hal-02531296

HAL Id: hal-02531296

<https://univ-rennes.hal.science/hal-02531296>

Submitted on 14 Apr 2020

HAL is a multi-disciplinary open access archive for the deposit and dissemination of scientific research documents, whether they are published or not. The documents may come from teaching and research institutions in France or abroad, or from public or private research centers.

L'archive ouverte pluridisciplinaire **HAL**, est destinée au dépôt et à la diffusion de documents scientifiques de niveau recherche, publiés ou non, émanant des établissements d'enseignement et de recherche français ou étrangers, des laboratoires publics ou privés.

Preparation and characterization of hollow silica nanocomposite functionalized with UV absorbable molybdenum cluster

Thi Kim Ngan Nguyen^{a,b,*}, Fabien Grasset^{a,b}, Stéphane Cordier^c, Maria Amela-Cortes^c, Yoshio Matsui^a, Naoki Ohashi^{a,b}, Naoto Shirahata^d, and Tetsuo Uchikoshi^{a,b,c,*}

^a Research Center for Functional Materials, National Institute for Materials Science (NIMS), 1-2-1 Sengen, Tsukuba, Ibaraki 305-0047, Japan

^b CNRS-Saint Gobain-NIMS, UMI3629, Laboratory for Innovative Key Materials and Structures (LINK), National Institute for Materials Science (NIMS), 1-1 Namiki, Tsukuba, Ibaraki, 305-0044, Japan.

^c Univ Rennes, CNRS, ISCR – UMR 6226, F-35000 Rennes, France

^d Research Center for Materials Nanoarchitectonics (MANA), National Institute for Materials Science (NIMS), 1-1 Namiki, Tsukuba 305-0044, Japan

Email address of coresonding authors:

Prof. Dr. UCHIKOSHI: UCHIKOSHI.Tetsuo@nims.go.jp,

Dr. NGUYEN: NGUYEN.Thikimngan@nims.go.jp.

Abstract

The nanoparticle-based material technology has recently opened a new heat shielding material generation for window applications such as aerogel, vacuum insulation panel or

nanospace materials. Aiming to prepare a nanospace-based heat insulation material functionalized with an ultraviolet (UV) absorbent, the Mo₆ cluster-deposited hollow silica nanoparticles (HSNs) were prepared by the vacuum impregnation process (VIP). The pore channels of the hollow silica wall filled with the Cs₂[Mo₆I₈(OCOC₂F₅)₆] octahedral cluster (CMIF) were confirmed by an HR-TEM coupled EDX device, ICP-OES and BET analysis. The retention of the octahedral structure or the typical optical property of the Mo₆ cluster in the pores of the HSNs was demonstrated by ultraviolet (UV) light absorption and photoluminescence spectroscopies even though the powders were heated to 200°C. The multi-functional CMIF@HSNs nanocomposite could adsorb the UV rays under 400 nm and scatter the NIR light through the pores of the silica wall in order to reduce the heat passing a window. For this purpose, the film preparation based on the CMIF@HSNs nanocomposite was performed by dip coating in the commercially available top coat suspension (TCS) on soda lime glass. Excellent mechanical and optical properties of the CMIF@HSNs-based thin film were visibly obtained with a relative transmittance. This study suggests a potential insulation material prepared by a high efficiency and simple method for reducing the air temperature in buildings.

Keywords: vacuum impregnation, hollow silica, luminescence, molybdenum cluster, thermal insulation.

1. Introduction

The efficient and advantage fabrication of thermal and electrical insulators has been a target of studies for energy saving applications that attempts to reduce the use of natural resources and greenhouse gas emissions [1, 2]. Nowadays, beside the use of the traditional thermal insulation materials with their restricted heat shielding efficiency [3], the remarkable

nanotechnology-based materials have been widely applied as vacuum insulation panels (silica, open porous or vacuum), aerogels, nano-ceramic thermal insulation coating or expanded polystyrene including a graphite powder additive to provide a prominent thermal insulation efficiency [4]. Among the nano-structured material generations for the thermal insulating applications, mesoporous silica nanoparticles have been the focus as a potential candidate for clean energy technologies [5], energy conversion and storage devices [6], and remarkably, with friendly environmental characteristics and biocompatibility [7]. For instance, the silica aerogel with its unique porous structure and chemical stabilization could adopt to many heat conducting conditions along with the proper photon scattering ability inside the pores [8]. However, the nanotechnology to prepare the silica aerogel is expensive which is the limitation in its use for bulk industrial production. Aiming to extend the actual efficiency, the transparent chemical-stabilized nanocomposites based on the hollow silica nanoparticles (HSNs) and polymers, such as polyethersulfone [9] or polyurethane [10], were attempted by means of the sol-gel or W/O emulsion process. The HSNs functionalized UV-cure polymer was also synthesized for a light diffuser film in liquid crystal display (LCD) applications [11]. The reasonable use of the HSNs as a heat absorbing component in the nanocomposite is due to the vibration of the molecules inside the nano-space accompanied by light scattering in the nano-sized pores during the irradiation that reduced the heat conductivity.

The heat conductivity of the mesoporous materials was demonstrated by three essential pathways through the solid materials, gas molecules and radiation through the pores [4, 12]. For the HSNs, these heat conducting mechanisms were prominently studied that involved the mesoporous spaces of the wall and big hollow. Therefore, the optimization of the high intrinsic capacity and specific surface area of the mesoporous HSNs with various shapes,

such as pseudocubes, ellipsoids, capsules, and peanuts, have been studied [13]. Aiming to extend the applicability of the HSNs, a chemical-stabilized polymer matrix has been used. Ernawati et al. reported a thermal insulation film exhibiting a low thermal conductivity ($0.03 \text{ W}\cdot\text{m}\cdot\text{K}^{-1}$) based on the hollow silica-blended polyethersulfone matrix [9]. In addition, Fuji et al. also claimed a hollow silica-polyurethane insulation film prepared by the sol-gel process that resulted in a decreased heat conductivity (0.029 W/mK) in comparison to the thermal conductivity of PU (0.18 W/mK), silica (1.180 W/mK) and air (0.024 W/mK) [10]. It is suggested that the heat was almost diffused inside the nano-spaces of the silica shells, followed by the heat shielding mechanism of the gas molecules and radiation through the pores and polymer matrix.

As is known, the $[\text{Mo}_6\text{L}^i\text{L}^a_8]^{n-}$ octahedral molybdenum cluster (L = Cl, Br, I with ⁱ as face-capping inner position and ^a as terminal apical position) has been formed on the octahedral block of the molybdenum transitional metal by metal – metal bonding. The Mo octahedral cluster unit neutralized by the electrostatic interaction with organic cations (NH_4^+ , ($n\text{-C}_4\text{H}_9$) $_4\text{N}^+$...) or alkali cations (Na, K, Cs...), exhibiting a strong absorption in the ultraviolet (UV) light range and organic luminescent properties has attracted much attention [14, 15]. Additionally, the light emission efficiency, one of the excellent properties of the Mo₆ cluster, depended on the electronic nature of the halogen ligands of the octahedral clusters and decreased from Cl, Br to I ligands [16]. The $\{\text{Mo}_6\text{I}_8^i\}^{4+}$ metallic core-enhanced luminescence efficiency by coordinating with the (OCOC₂F₅) functional group has been attempted to incorporate with polyurethane for use in an oxygen sensor [17], synthesize hybrid liquid crystals for electro-optic devices [18], fabricate with ZnO nanocrystals dispersed in a polyvinylpyrrolidone matrix [19] or prepare the cluster silica nanoparticles for time-gated luminescence bio-imaging [20]. It has been reported that the

toxicity of the $[\text{Mo}_6\text{Br}_8\text{Br}_6]^{n-}@\text{SiO}_2$ nanocomposite did not show any negative effect on the growth of plants [21] or harm to cells could be reduced by encapsulating the Mo_6 cluster in the silica nanoparticles [22]. Currently, the designing of the homogeneously spherical silica-based nanocomposites has mostly been carried out by the Stöber process [23, 24], water oil microemulsion, or sol-gel processing [25-29], with a high possibility of applying it in the laboratory but it is limited for a high productivity in industry.

In this study, the $\text{Cs}_2\text{Mo}_6\text{I}_8(\text{OCOC}_2\text{F}_5)_6$ cluster, exhibiting absorption in the UV light range and luminescent emission, was selected to be introduced into the pseudocube hollow silica nanoparticles (HSNs) by the vacuum impregnation process (VIP). The exchange of the apical ligands of the Mo_6 cluster by an aqueous solvent limited the usable solvent selection. Therefore, acetone was selected as the chemical-stabilized dispersing medium for the Mo_6 cluster and VIP coupled with thermal treatment was used to prepare the Mo_6 -functionalized HSNs. The pore of the hollow silica wall filled by the Mo_6 cluster was confirmed by HR-TEM coupled EDX, ICP-OES and BET analysis. The results of the UV-Vis-NIR absorption and photoluminescence spectra demonstrated that the optical properties of the Mo_6 cluster-functionalized HSN nanocomposites were still retained even when annealed at 200°C .

In the next step, a heat shielding film based on ultraviolet (UV) blocking absorbent-functionalized HSNs and coating polymer was prepared by dip coating on a soda lime glass with possible controlling of the thickness. A good adhesive mechanical morphology and excellent optical property based on quantum yield measurements have been obtained. The obtained heat shielding and UV band filter film based on the Mo_6 -incorporated hollow silica nanoparticle would be a promising heat insulation material in the future.

2. Material and methods

Materials

The $\text{Cs}_2\text{Mo}_6\text{I}_8(\text{OCOC}_2\text{F}_5)_6$ (CMIF) cluster was synthesized by the reaction of the $\text{Cs}_2\text{Mo}_6\text{I}_8\text{I}_6$ cluster, which resulted from the reaction of the MoI_2 and CsI_2 salts by the solid chemistry process [30], with the $\text{Ag}(\text{OCOC}_2\text{F}_5)$ salts by the solution chemistry process in the acetone solution. The apical I ligands of the $\text{Cs}_2\text{Mo}_6\text{I}_8\text{I}_6$ cluster were exchanged by the OCOC_2F_5 anions in the acetone medium with Ar gas in the dark for 48 h as reported in a previous study [18]. The AgI product or residual chemicals were almost eliminated in order to collect the pure orange-colored $\text{Cs}_2\text{Mo}_6\text{I}_8(\text{OCOC}_2\text{F}_5)_6$ cluster powder with the cluster unit size of 1.2 nm approximately.

The pseudocube hollow silica nanoparticles (HSNs, SiliNax SP-PN(b)), supplied from Nittestu Mining Co., Ltd, were synthesized using the calcium carbonate inorganic template [31]. The pore channel size (~ 5 nm) and BET surface area ($\sim 300 \text{ m}^2 \text{ g}^{-1}$) of the HSNs were characterized from the N_2 adsorption/desorption isotherm measurement (BELSORP-max II, Microtrac BEL Corp.). Considering the particle size of the HSNs, the surface area of $300 \text{ m}^2 \text{ g}^{-1}$ should be the sum of the outer and inner surfaces of the HSNs, indicating that the HSNs have open channels, the size of which is about 5 nm.

Vacuum impregnation procedure (VIP)

The cluster powder (2 g/L) and the HSNs (70 g/L) were optimally dispersed in reagent grade acetone (99.5 %, Nacalai Tesque, Inc., Kyoto, Japan) by agitating with a stirrer for 10 min to obtain homogeneous suspension before mixing together. The mixture suspension was placed in a vacuum chamber connected to a diaphragm pump creating the pressure of 0.1 Mpa (DAU-Z0, Ulvac Kiko, Inc). The HSNs was definitely impregnated in the Mo_6 cluster solution for 6 hours by VIP to obtain the dried powder which was heated at 60°C

for 30 minutes. This procedure was repeated in three times, and then last nanocomposite was completely washed and dried at 60°C for further use. The Mo₆ cluster structure and colorless washing suspension in acetone, the possible movement of the air or Mo₆ cluster solution, and deposition of the Mo₆ clusters on the HSNs are shown in Figure 1. The Mo₆ cluster and their nanocomposites were annealed at the different temperatures of 100°C, 150°C, 200°C for 30 min in air in order to confirm the thermal stability of the Mo₆ cluster-supported silica.

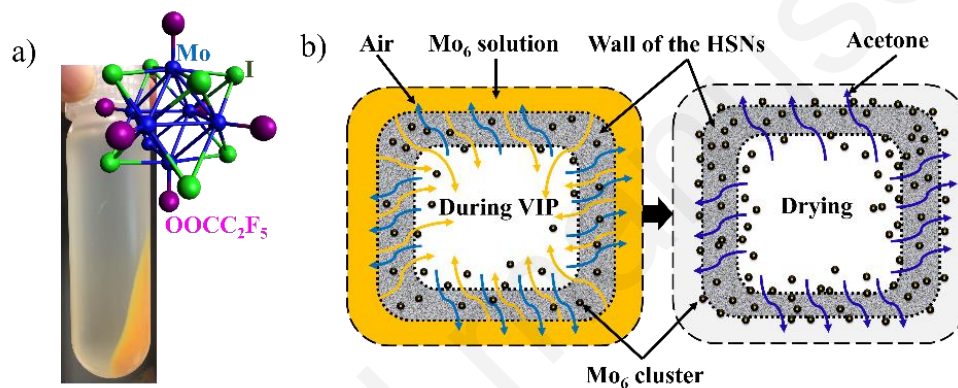


Figure 1. a) Mo₆ cluster schematic illustration and CMIF@HSNs suspension in acetone after 3 washings, b) the possible movement of the air and Mo₆ clusters during the VIP and the possible porosity structure of the HSNs deposited on the Mo₆ clusters.

The obtained CMIF@HSNs nanocomposite powder was dissolved in a nitro cellulose-based top coat solution (AC Nix Glossy, Dokubesu Co., Ltd., Tokyo, Japan) with acetone solvents by sonication for 2 minutes to obtain a homogeneous suspension. The ingredients of the top coat included the film former (nitro cellulose), thermoplastic resin (toluene sulfonamide formaldehyde resin), plasticizer (dibutyl phthalate), solvents and pigment. The CMIF@HSNs nanocomposite film was prepared by dip coating on soda lime glass (~1.5 mm, S1214, Matsunami Glass Ind., Ltd., Japan) for 3 times and 6 times at the

different nanocomposite powder concentrations of 2 g/L, 4 g/L and 6 g/L. The obtained nanocomposite film was dried at 60°C for 1 hours to obviously eliminate the solvent for further characterization.

The size, surface morphology and distribution of the HSNs and its nanocomposites were observed by a field-emission scanning electron spectroscopy (FE-SEM, Hitachi S4800) operated at 10 kV. A transmission electron microscope (TEM) and scanning transmission electron microscope (STEM) equipped with an EDX analysis device (JEOL JEM 2100F) were used to verify the existence of the Mo₆ clusters on the wall of the HSNs. Inductively coupled plasma optical emission spectrometry (ICP-OES, Agilent 720-ES) coupled with ion-chromatography (Thermofisher Scientific ICS-1600) was used to verify the element concentration of the samples. An FTIR spectroscopy (ThermoScientific Nicolet 4700) was used to determine the difference in the chemical components of the HSNs, Mo₆ clusters and its nanocomposite. The powder was mixed and ground with KBr powder as the baseline and the measurement was performed in the wavenumber range between 4000 cm⁻¹ and 400 cm⁻¹. The patterns of the CMIF and CMIF@HSNs were identified by an X-ray diffraction (XRD) measurement (Altima 3, Rint 2000, Rigaku Corp.) at 40 kV and 30 mA in the 2θ angle range from 5 to 55° with Cu Kα radiation (λ = 0.15405 nm). The reflection and UV-Vis-NIR absorption spectra of the HSNs and its nanocomposites were measured by a UV-Vis-NIR spectroscopy (V570, Jasco Corp.) in the wavelength range between 1000 nm and 200 nm with the scan rate at 400 nm/s. The photoluminescence (PL) was measured by a micro PL system (Lab Ram HR, Horiba Corp.) with a 325-nm He-Cd laser system. The nitrogen adsorption isotherm according to the BET model of the HSNs and CMIF@HSNs nanoparticles was performed in a saturated vapor pressure of about 100 kPa at the temperature of 140°C for 2 days (BELSORP-max II, Microtrac BEL Corp.). The

quantum yield was measured by an absolute PL quantum yield spectrometer C11347 (Hamamatsu Corp.) in the wavelength range between 250 nm to 850 nm created by a 150W xenon lamp light source. The droplet and surface adhesion testing was captured by a digital microscope (VHX-600, Keyence Co., Ltd.) with a 20X magnification. The thickness of the obtained nanocomposite films was measured by a high-resolution color 3D laser microscope (VK-9700, Keyence Co., Ltd.) with a 408-nm wavelength laser light. The adhesion test of the nanocomposite film followed the standard test methods of D 3359 – 97 (test method B) by transparent tape (Cellophane No. 252, 0.049 mm, adhesion strength of 3.1 N/10 mm, tensile strength of 36 N/10 mm, Sekisui Chemical Co., Ltd., Japan).

3. Results and discussion

Characteristic of the Mo₆ cluster-functionalized silica nanoparticle

For the first time, the VIP was used to introduce the Mo₆ cluster into hollow silica nanoparticles (HSNs) under ambient conditions. Many of the nano-channels in the shell of the HSNs are about 5 nm in diameter that is a good pathway to push the nanocluster under the impact of low air pressure (0.1 MPa). The selection of a good cluster dispersing medium is also important to limit the exchange of the apical ligand by aqueous molecules, prepare the suitable sized particle for entering the pore channels and able to stabilize the chemical property of the HSNs. For these reasons, acetone is an excellent cluster dissolving solvent and can reduce the physical or chemical interaction with the HSNs. The drying process at 60°C was alternatively combined with the impregnation process for every step that accelerated the evaporation of the solvent, followed by coagulation of the clusters which were trapped in the pores of the HSNs. The efficiency of the cluster introduction was

enhanced when air was completely replaced by the Mo_6 solution during the VIP and the total evaporation of acetone during the drying process.

In order to consider the efficiency of the VIP method, a CMIF@HSNs was prepared without the control of the VIP. The mixture of the CMIF and HSNs dispersed in acetone was continually agitated for 6 hours, then purified 3 times in acetone without the VIP. The obtained reflectance results in the UV-Vis light range of the samples are shown in Figure 2a. The color of the nanocomposite prepared by a simple solution stirring without using the VIP is mostly white as a color of the pure silica meanwhile a yellow-colored nanocomposite was achieved by the VIP method. The low reflectance in the visible light range was observed for the CMIF and CMIF@HSNs . By using the VIP, the CMIF cluster strongly tends to fulfill the pores on the outside wall of the HSNs that obviously absorbs the UV-Vis light, resulting in a decrease of the reflectance light in the light range between 300 nm and 600 nm. The higher reflectance possibly corresponds with a low optical absorption. The Mo_6 cluster (CMIF) presents a strong absorption in the range between 400 and 550 nm of visible light. The absorption tendency in the visible light range depends on the nature of the apical ligand. The decrease in the apical ligand (OCOC_2F_5) groups by exchange with the solvent or OH group from the silica matrix causes a decrease in the optical absorbing nature of the CMIF@HSNs in this range. As is known, the photoluminescence characteristic origins come from the molybdenum octahedral structure coordinating with halogen ligands [14, 15, 17]. The Mo_6 octahedral clusters obviously trapped on the wall of the HSNs were also indicated by the photoluminescence behavior as presented in the CMIF (Fig. 2b). Moreover, the interaction of the cluster and HSNs was found through the shift in the photoluminescence peak from 666 to 676 nm for the CMIF@HSNs . This obtained result was similarly recognized in a previous report. It was

suggested that the hydrogen bonds and covalent bonds could be formed between the cluster units and silica matrix which caused a shift in photoluminescence spectrum [21].

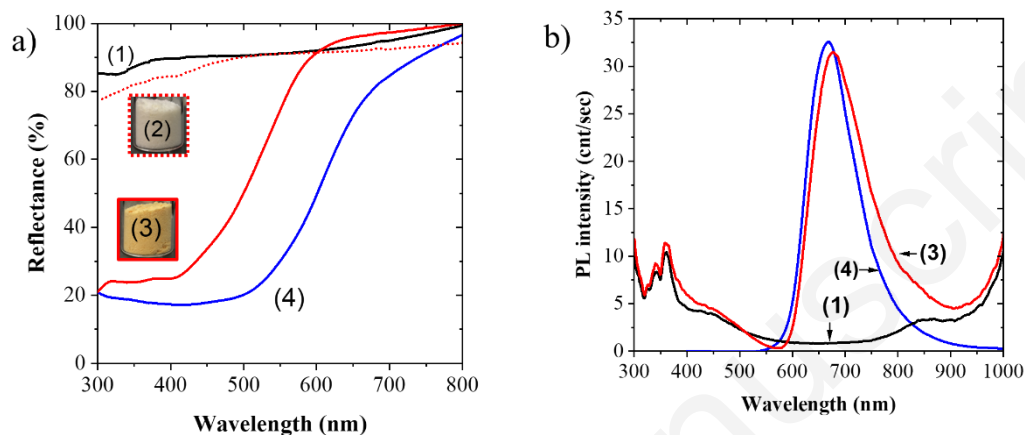


Fig 2. a) The reflection spectra in the UV-Vis light absorbing range and b) photoluminescence spectra of: 1) HSNs, 2) CMIF@HSNs by mixing without the VIP, 3) CMIF@HSNs with the VIP and 4) the CMIF.

Aiming to confirm the efficiency of the solvent and heat treatments on the morphology and distribution of the pseudocube HSNs, the FE-SEM observations of the CMIF and CMIF@HSNs were performed as seen in Figure 3. Normally, the CMIF cluster exhibits condensed crystals with bulk sizes (Fig. 3a) and the pseudocube shape of the HSNs still retains the perfect pseudocube shape after treatments with the acetone solution by the VIP for 18 hours (Fig. 3b). The bulk size of the metal cluster crystals does not involve the outside shell or the space between of the HSNs. It is known that the CMIF cluster is strongly associated in the acetone solution to break the bulk block. Additionally, the acetone solution seems to be the best choice to prepare the nanocomposite because it does not destroy the Si-O-Si linking on the wall of the silica nanoparticles.

The observations were performed by HR-TEM and STEM coupled with an EDX analysis device to recognize the existence of the Mo_6 cluster and its deposited position on the HSNs. The pseudocube shape of the HSNs existing in the internal cavity with the size of about 50 nm is recognized in the HR-TEM image, followed by the wall thickness of about 10 nm (Fig. 3c). The STEM image of the CMIF@HSNs shows clear white dots on the HSNs area (Fig. 3d) which are assigned to the Mo_6 cluster with the minimal size of about 1 nm obviously incorporated in the shell pores of the HSNs. Moreover, the overlapped EDX mapping of the CMIF@HSNs definitely demonstrates evidence of the Mo element on the HSNs that strongly proves the confirmation of the Mo_6 deposition (Fig. 3e).

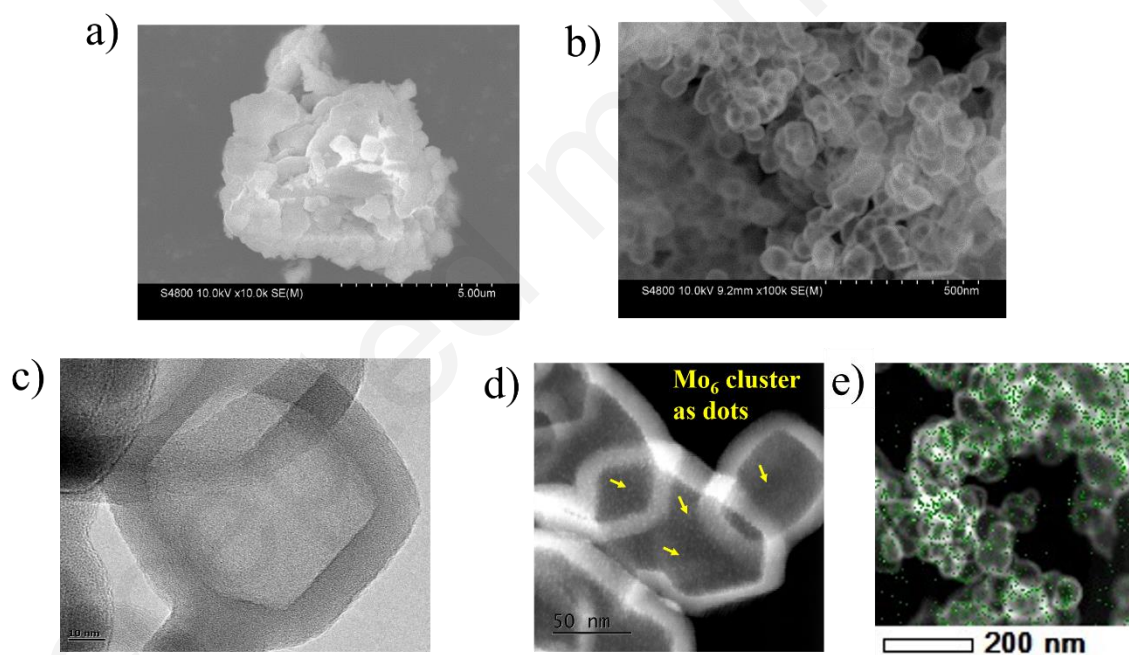


Figure 3. FE-SEM images of: a) CMIF cluster, b) CMIF@HSNs, HR-TEM image of: c) the HSNs, d) STEM image of CMIF@HSNs, and e) the overlapped EDX mapping image of the Mo element on the HSNs.

The atomic ratios of the CMIF and CMIF@HSNs were measured by an FE-SEM coupled

with an EDX analyzer and presented in Table 1. Following the EDX technique, most of the elements on the surface starting from the 10-nm wall thickness will be determined. The ratios of the Cs, Mo, Cl, I and F atoms of the CMIF cluster are close to the theoretical index. The inner and apical atoms of the CMIF cluster exhibit a slight difference from the theoretical index because the exchange reaction between the I⁻ anion and (OCOC₂F₅)⁻ anion could not be completely performed. In addition, it is suggested that the residual CsI agents have not been completely eliminated from the last CMIF powder product. The optical property of the octahedral Mo₆ cluster originates from the d orbitals of the Mo atoms which forms the octahedral structure and is affected by the nature of the apical ligand [18]. For this reason, CsI does not participate in the octahedral structure of the Mo₆ cluster, thus having no effect on the optical property of the CMIF or CMIF@HSNs [27]. In the case of the CMIF@HSNs, the value of the Cs atoms slightly increases as it is absorbed on the negative charged surface of the HSNs. Simultaneously, the decrease in the F atoms corresponds to the loss of two (OCOC₂F₅)⁻ groups at the terminal apical position by the exchange of the ligands. Moreover, the atomic ratio of Si and Mo performed by ICP-OES analysis was measured to be about 82 that confirmed the successful Mo₆-cluster introduction in the HSNs.

The prediction is that the (OCOC₂F₅) groups on the [Mo₆I₈(OCOC₂F₅)₆]²⁻ cluster could be associated following the mechanism of the acid catalyzed hydrolysis of the esters [32] in the presence of the hydroxonium ion which is generated from the proton transformation of the keto-enol tautomerism in the acetone-water solution [33] or from the hydroxo groups of the HSNs. The pH of the mixture solution which was found to be about 5 also supports this suggestion. The predicted products would be C₂F₅COOH, C₂F₅CO-O-Silica and [Mo₆I₈(OCOC₂F₅)_{6-x}(H₂O)_x]^{2-x} or [Mo₆I₈(OCOC₂F₅)_{6-x}(OH)_x]²⁻ clusters which were

immobilized on the HSNs by hydrogen bonding or a covalent bond (Mo-O-Si) as suggested in a previous report [21].

Table 1. The atomic ratio of the Cs, Mo, Cl, I, F and O elements in the CMIF cluster and CMIF@HSNs measured by an FE-SEM coupled with the EDX analyzer. The data of the other elements were calculated from the Mo atom % of 6. *Theoretical atomic composition was calculated based on the formulation of the $Cs_2Mo_6I_8(OCOC_2F_5)_6$ cluster unit.

Sample	Mo (%at)	I (%at)	F(%at)	Cs (%at)
CMIF*	6	8	30	2
CMIF	6.0	9.5±0.2	28±2	2.1±0.1
CMIF@HSNs	6.0	7.0±0.2	20±1	2.3±0.1

The chemical bonding characteristic of the samples measured by the FTIR spectroscopy is presented in Figure 4a. For the HSNs, the absorption bands of the O-H stretching vibration in the wavenumber range between 3600 and 3200 cm^{-1} , H-O-H bending vibration at 1632 cm^{-1} and Si-O-Si bending vibration in the range between 1200 and 1000 cm^{-1} are recognized. The FTIR spectrum of the CMIF cluster shows the strong and sharp absorbing peaks at the wavenumber of 3500 cm^{-1} assigned for the O-H stretching vibration and 1608 cm^{-1} assigned for the H-O-H bending vibration of a water molecule [34], and 1690 cm^{-1} assigned to the C=O stretching vibration from the $(OCOC_2F_5)$ apical group. It also includes the absorption bands of the C-O-C bending vibration in the range between 1300 and 1000 cm^{-1} and C-F stretching vibration in the range between 800 and 500 cm^{-1} assigned to the $(OCOC_2F_5)$ apical group. In the case of the CMIF@HSNs nanocomposite, most of the

absorption bands are similar to the FTIR spectrum of the HSNs. A small shoulder peak at the wavenumber of 1690 cm^{-1} (C=O) in the spectrum of the CMIF@HSNs could indicate the existence of the CMIF cluster.

The XRD pattern diagrams of the CMIF and CMIF@HSNs show the modification of the $\text{Cs}_2\text{Mo}_6\text{I}_8(\text{OCOC}_2\text{F}_5)_6$ pattern after the introduction of the CMIF (Fig. 4b). Based on the association and impregnation processes in the solvent, the original crystallographic pattern of the CMIF is difficult to recognize, resulting in the disappearance of the specific peaks in the curve of the CMIF@HSNs nanocomposite. This is also in agreement with the SEM and STEM images. The XRD result proves the preparation of a good homogeneous nanocomposite with the nanoparticles of the CMIF using acetone.

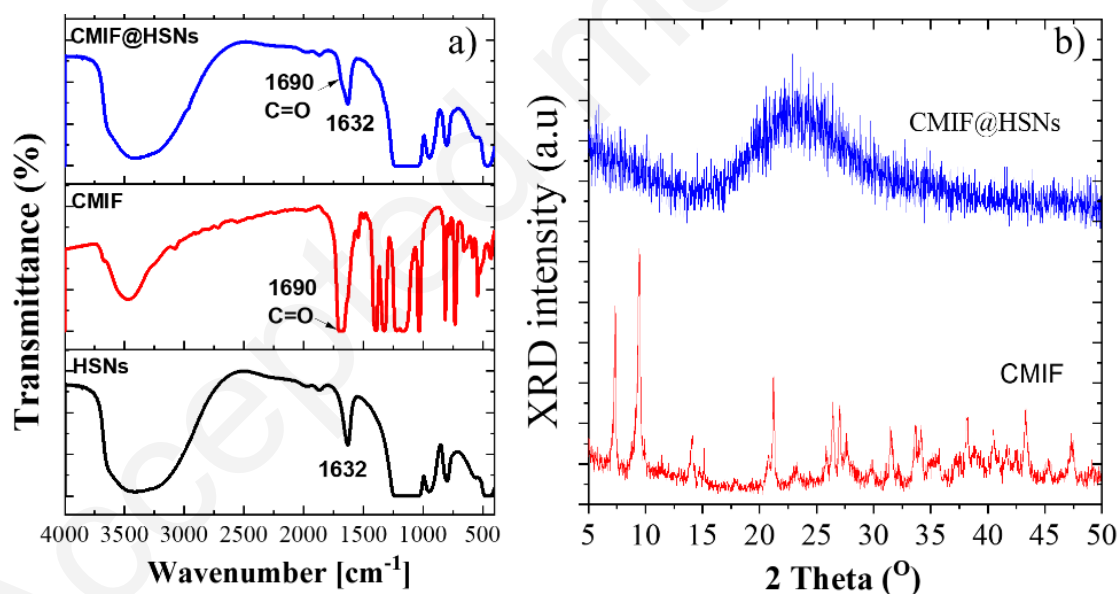


Figure 4. a) FTIR spectra and b) The powder XRD pattern diagrams of the CMIF cluster, HSNs and CMIF@HSNs.

The mean pore diameter distributions and nitrogen (N_2) adsorption-desorption isotherms

according to the BET model of the HSNs and CMIF@HSNs nanocomposite are shown in Figure 5. It can be seen that the peak diameter of the main pore channel is about 5 nm for the HSNs, while it almost disappears after the introduction of the Mo₆ clusters (Fig. 5a). The specific surface areas of the HSNs and CMIF@HSNs were 296.7 and 106.2 m²g⁻¹, respectively, that could essentially originate from the volume inside the pores and the hollow. The remarkable decrease of the BET surface area enhances the suggestion of the deposition of the tiny Mo₆ clusters in the pores of the silica wall. Moreover, the large void between the silica nanoparticles negligibly changes illustrates no coalescence of the silica nanoparticles after the treatment of the VIP. The shape of the nitrogen adsorption-desorption isotherm curve of the HSNs and CMIF@HSNs was also demonstrated in Figure 5b that definitely agrees with the theoretical adsorption isotherm curve for the porous material. From the Nitrogen adsorption-desorption isotherms of the porous HSNs, it can be seen that the total volume of the pore significantly reduces after depositing the Mo₆ cluster. Moreover, N₂ gas seems to be difficult to go into the HSNs via the narrow pore channels of the HSNs during the measurement processed at 140°C. This phenomenon has not been observed for the CMIF@HSNs since the pore channels are clogged with the Mo₆ cluster nanoparticles.

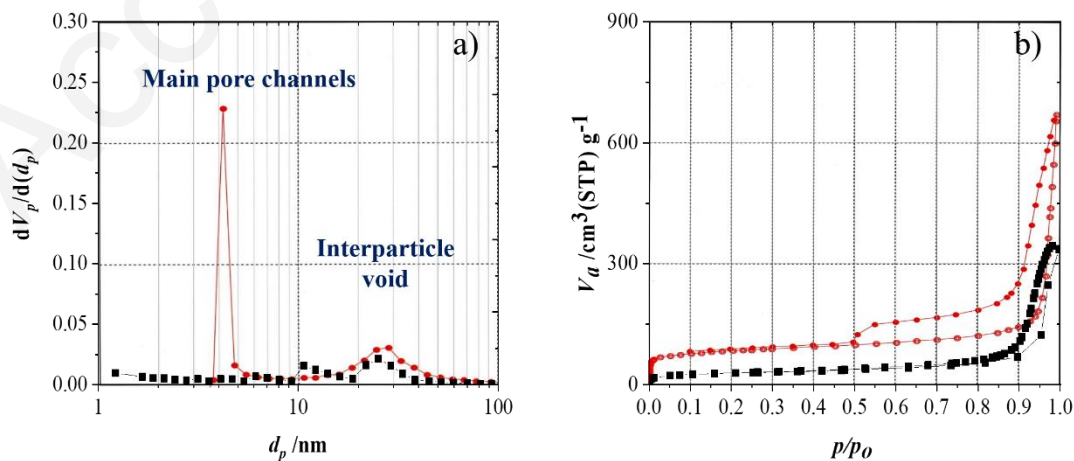


Figure 5. a) BJH pore size distribution plots and b) Nitrogen adsorption-desorption isotherms according to the BET model of the HSNs (circle) and CMIF@HSNs (square).

The optical property stabilizing ability of the Mo₆ cluster-based silica nanoparticles

The optical property, such as the photoluminescence and UV-Vis absorption, will confirm the retention of the octahedral structure of the Mo₆ cluster after the VIP shown in Figure 6a. The optical characteristic depends on the Mo₆ octahedral structure with specific ligands that determines the UV-Vis light absorption and the luminescent emission in the NIR range. The chemical interaction between the Mo₆ cluster and the HSNs has obviously been seen before. Vorotnikov et al. suggested some mechanisms and interactions which can occur between the hydrolyzed Mo₆ cluster unit and functional groups anchoring on the surface of the silica nanoparticles by the W/O emulsion process. It is predicted that the hydrolysis of the Mo₆ cluster units to form aquahydroxo or hydroxo cluster units that interact with the silica nanoparticles by hydrogen bonding and covalent linking form the compound with the general formula $[\{\text{Mo}_6\text{X}_8\}(\text{H}_2\text{O})_{6-y-z}(\text{OH})_y(\text{OSi})_z]_{4-y-z}$ [35]. With the excellent interaction between the CMIF and HSNs components, the UV-absorbing possibility of the CMIF component definitely resulted in the CMIF@HSNs. In addition, the optical absorbing ability of the nanocomposite does not change when it is heated to 200°C. This thermal stability originates from the duration of the nanostructured-Mo₆ cluster even with of the interaction with the functional group that occurs on the surface of the HSNs.

Besides the prominent optical absorption characteristic, the luminescent emission is also a significant property of the CMIF@HSNs nanocomposite. The stability of the luminescent emission increases its possible uses. In this study, the HSNs, CMIF and CMIF@HSNs annealed at 60°C, 100°C, 150°C, and 200°C for 30 minutes had the photoluminescence

measured during irradiation at 325nm by laser light as shown in Figure 6b. The HSNs obviously displays a slight emission at the wavelength of 850 nm while the CMIF cluster exhibits a strong emission in the wavelength range between 550 and 900 nm with the maximum peak at the wavelength of 668 nm. The essential emission of the CMIF@HSNs nanocomposite annealed at 60°C involves the partial emission of the HSNs and CMIF cluster though the PL intensity was low because of the residual liquid. However, the emitting peak shifts from 668 nm to 680 nm accompanying the extension of the wavelength range higher than 800 nm corresponding to the appearance of the shoulder peak at 850 nm which is assigned to the HSNs. The optical property of the CMIF@HSNs prepared by the VIP demonstrates the same behavior seen in previous studies prepared by the W/O micro-emulsion process [20, 21]. When the annealing temperature was raised to 200°C, the intensity of the emission peak of the CMIF at 688 nm gradually decreased after it reached the highest intensity at 100°C. Based on this result, the drying temperature at 100°C is necessary to completely eliminate the trapped water or acetone molecules inside the silica nanoparticles. In summary, the CMIF@HSNs nanocomposite can retain the optical properties when even annealed at 200°C that appears impressive in comparison to the perovskite quantum dots-coated silica by in situ synthesis exhibiting an optical stability under 125°C [36]. With the purpose to use as a thermal resistant insulation material, the CMIF@HSNs nanocomposite would be a promising candidate due to the strong UV light absorbing, radiation and scattering the NIR light in the pores and big hollows of the HSNs, and possibly be used at high temperature. These characteristics will be an advantage to possibly reduce the air temperature in buildings for energy saving applications.

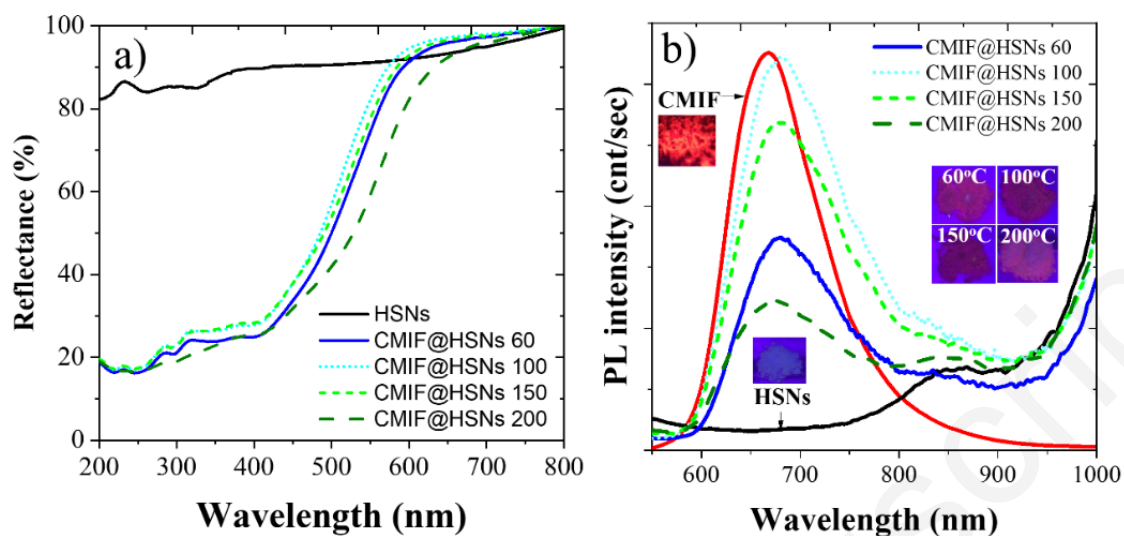


Figure 6. a) The UV-Vis absorption and b) the photoluminescence spectrum of the CMIF cluster and CMIF@HSNs after VIP at 60°C and annealed at 100°C, 150°C, and 200°C for 30 min in air.

The mechanical and optical properties of the CMIF@HSNs-based film

A hydrophobic CMIF@HSNs-based designed film was prepared by the dip coating method using the nitrocellulose-based top coating solution (TCS) as a stabilized matrix deposited on soda lime glass slides. The hydrophobic nanocomposite films assigned from F1 to F5 with different thicknesses were prepared from various concentrated solutions. The soda lime glass was immersed in the nanocomposite suspension for 3 or 6 times, then dried at 60°C for 1 hour to form the CMIF@HSNs film corresponding to the increased thickness (Tab.2 and Fig. 7a). For the adhesion measurement with tape, the films were cut 1 mm apart and eleven cuts made to form the patterns on the surface as shown in Figure 7c. It can be seen that the destruction of the film surface was not observed after testing the adhesion with tape, followed by the 4B~5B classification of the ASTM D3359-97 standard test method that showed an excellent mechanical property (Fig. 7c). In summary, the TCS is a

good dispersing media for the CMIF@HSNs, and the dip coating method is one of the efficient and simple methods to obtain the CMIF@HSNs thin film with a high mechanical property.

Table 2. The concentrations of the CMIF@HSNs powder in TCS and the thickness of the CMIF@HSNs films.

Sample	CMIF@HSNs in TCS (g/L)	Number of dip	Thickness (μm)
F1	2	3	3.1 ± 0.5
F2	2	6	4.6 ± 0.7
F3	4	3	4.5 ± 0.6
F4	4	6	5.9 ± 1.5
F5	6	3	4.5 ± 0.9

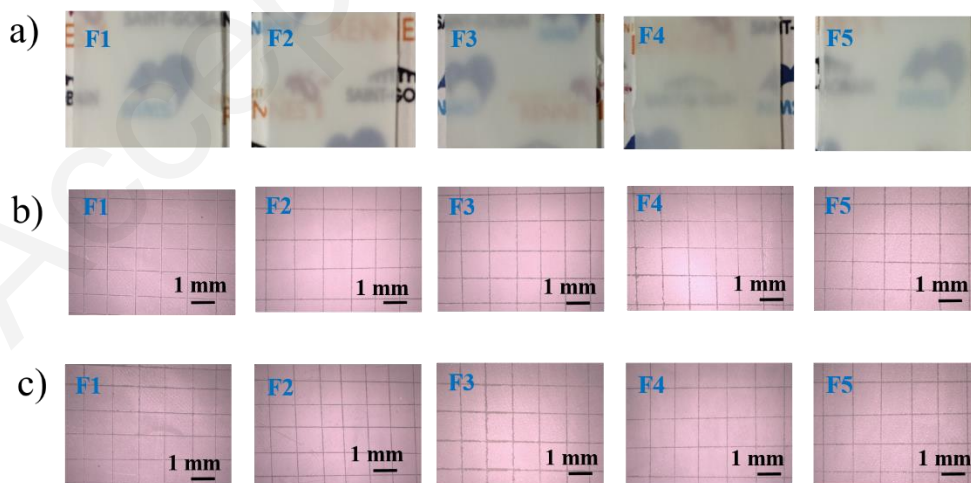


Figure 7. a) Photos of the CMIF@HSNs films prepared by dip coating with different

nanocomposite powder concentrations and dipping numbers under visible light. The morphology of the film by microscope b) after cut to form the patterns on the surface and c) The cut film after tested by adhesion measurement using tape.

The morphology of the pure top coat film (F0 with 3 dips) and hydrophobic property the CMIF@HSNs based films (F1~F5) were observed using a color 3D laser microscope (Fig. 8). The F0 film appears to have many uniform spherical holes on the surface that causes the strong scattering by the film, consequently, the film is not transparent. Similarly, the porous morphology is recognized for most of the CMIF@HSNs films from the F1 film to F5 films. However, the homogeneity of the film is reduced and the size of the holes increased when an increase in the number of dips. The compatibility of the nanocomposite and TCS in acetone influences the homogeneity of the obtained films. At a high concentration, the surface become rougher due to a non-uniform distribution of the CMIF@HSNs nanoparticles over the whole film. The hydrophobic characteristic was determined by the contact angle which was calculated from the water droplets captured on the surface of the film. Normally, the soda-lime glass used as a coating film has a contact angle lower than 90° or obtains a hydrophilic surface as seen in Figure 8. The contact angles of the films (F0~ F5) have values greater than 90° which means all the films achieve a hydrophobic characteristic. The existence of the CMIF@HSNs nanoparticles does not influence the waterproof property of the F0 film because the hydroxyl groups existing on the surface of the HSNs nanoparticles have been protected by TCS from the water. It is predicted that the hydroxyl groups on the HSNs are blocked by the Mo_6 cluster or the ingredients of the TCS. The excellent waterproof characteristic of the cluster@HSNs films is one of the prominent advantages for applications involving harsh weather conditions.

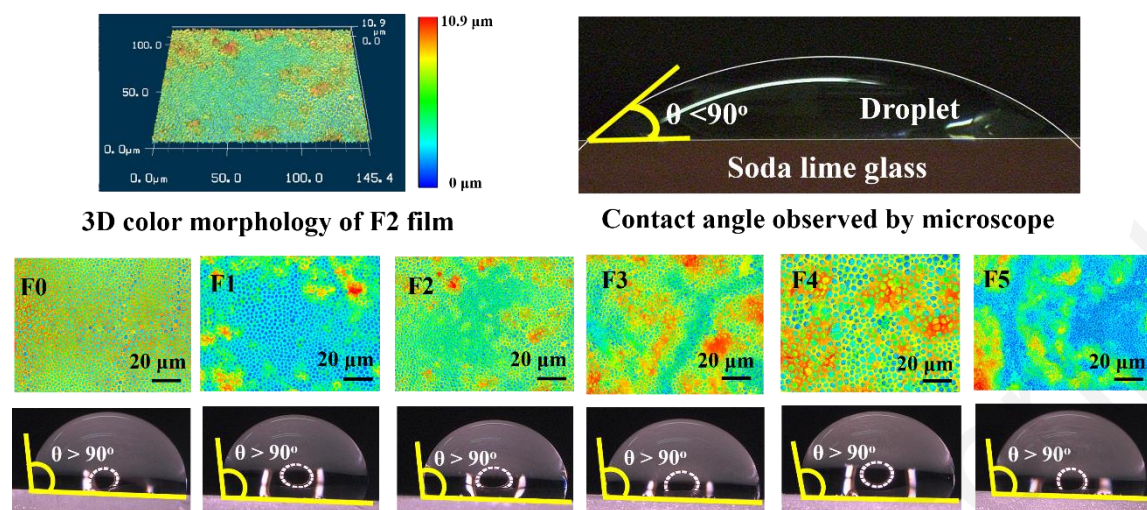


Figure 8. The 3D color morphology of the CMIF@HSNs nanocomposite films (up) and water droplet photos for calculating the contact angle (down).

The photos of the nanocomposite films show a red light emission during the irradiation of UV light at 365 nm as shown in Figure 9. The brightness of the red emitting color is strongly improved when the thickness or concentration of the CMIF@HSNs nanocomposite in the film increase. The F1, F3, and F5 exhibiting a relative thickness (3~5 μm) were selected to measure the PL quantum yield (PL QY) by the excitation at the wavelength between 300 nm and 600 nm. The CMIF cluster obtained an excellent PL QY in the excited wavelength between 400 nm and 500 nm with the maximum quantum yield of about 26%. However, the PL QY of the Mo₆ cluster significantly decreased when it was incorporated with the HSNs corresponding with the maximum PL QY reaching 18% during excitation at the wavelength of 420 nm. In HR-TEM image and EDX mapping, the Mo₆ clusters are almost condensed in the pore channels of the walls of the HSNs.

During the irradiation on the mesoporous CMIF@HSNs powder, the increase in the light absorbing intensity partially originated by the CMIF cluster and the simultaneous decrease of the light emitting intensity caused by the scattering inside the pores of the HSNs suggests

the reason for the decrease in the PL QY [37]. The CMIF still retains the low intensity PL QY at the excitation wavelength of 600 nm while it disappears in the CMIF@HSNs powder. The metal cluster in the pore channels of the HSNs acts as an UV light absorbing agent and the photon energy is immediately consumed by transferring to the emitting state. In addition, the nano-space structured HSNs will diffuse the emitting light and NIR light by the scattering behavior inside the pores. In the nanocomposite film, PL QY was significantly reduced due to the enhanced light scattering inside the holes which is generated from the top coat suspension. When the emitting light scattering in the nanocomposite film strongly occurs, the emission intensity from the CMIF is reduced. For this result, the porous nanocomposite film can eliminate the negative effect from the UV light and heat from the NIR light for window applications.

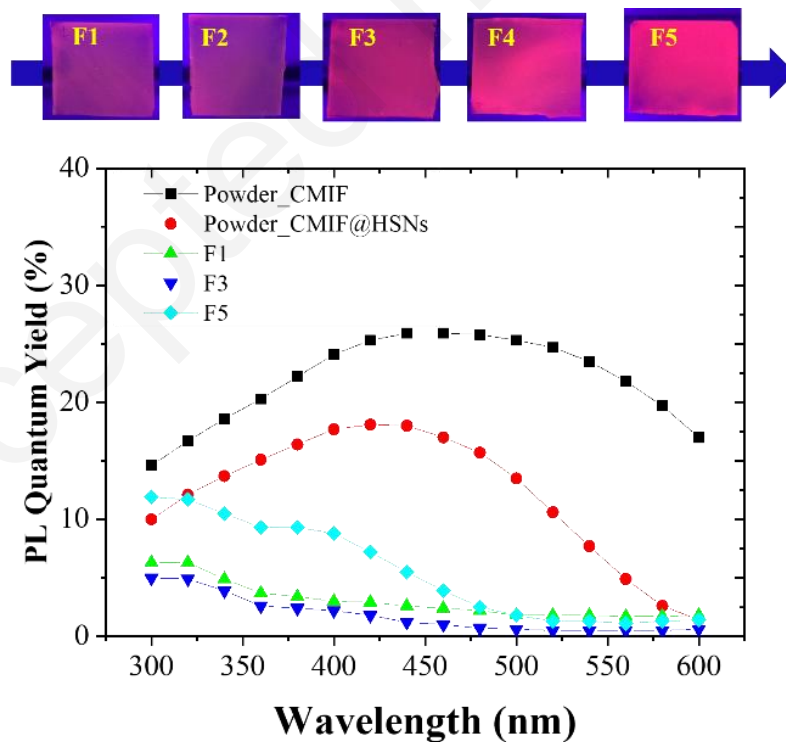


Figure 9. The red light emitting photos of the CMIF@HSNs films with different concentrations and coating process excited by 365 nm UV light and the PL QY of the CMIF, CMIF@HSNs powder and CMIF@HSNs films.

4. Conclusions

The Mo₆ octahedral cluster-functionalized HSNs have been successfully synthesized by the vacuum impregnation process (VIP) at room temperature. The morphology and shape of the HSNs and optical property of the Mo₆ octahedral cluster have been visibly retained after solvent and thermal treatment in an organic dispersing medium as well as the optical property of the Mo₆ cluster medium. Based on the FE-SEM and HR-TEM measurements, the existence and distribution of the Mo₆ cluster inside the pores of the HSNs shell were determined. The stabilization of the prominent optical property of the CMIF@HSNs nanocomposite is obviously observed until annealing to 200°C by the demonstration of the UV-Vis absorption and PL spectra. The hydrophobic and prominent luminescent CMIF@HSNs films fabricated on the soda lime glass were studied. The PL quantum efficiency of the CMIF@HSNs nanocomposite is lower than that of the cluster itself because the emitting light scatter strongly occurs in the pores of the silica wall and inside the film coat. The insulation characteristic of the CMIF@HSNs film exhibiting the heat diffusing property caused by the NIR light in the porous channel of the HSNs and the possible blocking of the UV light by the Mo₆ cluster strongly suggests a material for window applications.

Acknowledgements

This study was carried out as part of the France-Japan international collaboration

framework through the Laboratory for Innovative Key Materials and Structures (UMI3629 – ICC Center). The study was financially supported by the National Institute for Materials Science (NIMS), Saint-Gobain (France), CNRS and Université de Rennes 1 (UMR 6226). The authors wish to thank David Lechevalier and Dr. Mari Kono of Saint-Gobain KK (Tokyo, Japan) involved in LINK and related activities. We would like to thank Noée Dumait for the synthesis of metal cluster and Ms. Takazawa at NIMS for her help with the PL quantum yield measurements.

References

- [1] S. Schiavoni, F. D. Alessandro, F. Bianchi, F. Asdrubali, Insulation materials for the building sector: A review and comparative analysis, *Renewable and Sustainable Energy Reviews*, 62 (2016) 988-1011.
- [2] T. Ojanena, I. P. Seppää, E. Nykänena, Thermal insulation products and applications - Future road maps, *Energy Procedia*, 78 (2015) 309 - 314.
- [3] F. Asdrubali, F. D'Alessandro, S. Schiavoni, A review of unconventional sustainable building insulation materials, *Sustainable Materials and Technol.*, 4 (2015) 1-17.
- [4] D. Bozsaky, Application of nanotechnology-based thermal insulation materials in building construction, *Slovak J. Civil Engi.*, 24 (2016) 17 - 23.
- [5] N. Linares, A. M. Silvestre-Albero, E. Serrano, J. Si. Albero, J. G. Martinez, Mesoporous materials for clean energy technologies, *Chem. Soc. Rev.*, 43 (2014) 7681-7717.
- [6] W. Li, J. Liu, D. Zhao, Mesoporous materials for energy conversion and storage devices. *Nature Rev. Mater.*, 1 (2016) 1-17.
- [7] R. Mitran, D. Berger, C. Munteanu, C. Matei, Evaluation of Different Mesoporous Silica Supports for Energy Storage in Shape-Stabilized Phase Change Materials with

- Dual Thermal Responses, *J. Phys. Chem. C*, 119 (2015) 15177–15184.
- [8] M. A. Hasan, R. Sangashetty, A. C. Mary Esther, S. B. Patil Baburao, N. S. Dey, Prospect of thermal insulation by silica aerogel: A brief review, *J. The Institution of Engineers (India): Series D*, 98 (2017) 297-304.
- [9] L. Ernawati, T. Ogi, R. Balgis, K. Okuyama, M. Stucki, S. C. Hess, W. J. Star, Hollow silica as an optically transparent and thermally insulating polymer additive, *Langmuir*, 32 (2016) 338–345.
- [10] M. Fujia, C. Takai, H. Watanabe, K. Fujimoto, Improved transparent thermal insulation using nano-spaces, *Advanced Powder Technol.*, 26 (2015) 857-860.
- [11] W. Suthabanditpong, C. Takai, M. Fuji, R. Bunttem, T. Shirai, Improved optical properties of silica/UV-cured polymer composite films made of hollow silica nanoparticles with a hierarchical structure for light diffuser film applications, *Phys. Chem. Chem. Phys.*, 18 (2016) 16293-16301.
- [12] T. W. Tong, D.L. McElroy, D.W. Yarbrough, Transient conduction and radiation heat transfer in porous thermal insulations, *J. Building Phys.*, 9 (1985) 13-29
- [13] Y. Wang, X. Su, P. Ding, S. Lu, H. Yu, Shape-Controlled Synthesis of Hollow Silica Colloids, *Langmuir*, 29 (2013) 11575–11581.
- [14] K. Kirakci, S. Cordier, C. Perrin, Synthesis and characterization of $\text{Cs}_2\text{Mo}_6\text{X}_{14}$ (X = Br or I) hexamolybdenum cluster halides: efficient Mo_6 cluster precursors for solution chemistry syntheses, *Z. Anorg. Allg. Chem.*, 631 (2005) 411-416.
- [15] G. Saito, H. Hosoda, Y. Yoshida, J. Hagiwara, K. Nishimura, H. Yamochi, A. Otsuka, T. Hiramatsu, Y. Shimazaki, K. Kirakci, S. Cordier, C. Perrin, Synthesis and properties of charge-transfer solids with cluster units $[\text{Mo}_6\text{X}_{14}]^{2-}$ (X= Br, I), *J. Mater. Chem.*, 22 (2012) 19774-19791.

- [16] J. A. Jackson, C. Turro, M. D. Newsham, D. G. Nocera, Oxygen quenching of electronically excited hexanuclear molybdenum and tungsten halide clusters, *J. Phys. Chem.*, 94 (1990) 4500-4507
- [17] M. A. Cortes, S. Paofai, S. Cordier, H. Folliot, Y. Molard, Tuned red NIR phosphorescence of polyurethane hybrid composites embedding metallic nanoclusters for oxygen sensing, *Chem. Commun.*, 51 (2015) 8177-8180.
- [18] M. Prévôt, M. A. Cortes, S. K. Manna, R. Lefort, S. Cordier, H. Folliot, L. Dupont, Y. Molard, Design and integration in electro-optic devices of highly efficient and robust Red-NIR phosphorescent nematic hybrid liquid crystals containing $[\text{Mo}_6\text{I}_8(\text{OCOC}_n\text{F}_{2n+1})_6]^{2-}$ ($n = 1, 2, 3$) nanoclusters, *Adv. Funct. Mater.*, 25 (2015) 4966-4975.
- [19] T. G. Truong, B. Dierre, F. Grasset, N. Saito, N. Saito, T. K. N. Nguyen, K. Takahashi, T. Uchikoshi, M. Amela-Cortes, Y. Molard, S. Cordier, N. Ohashi, Visible tunable lighting system based on polymer composites embedding ZnO and metallic clusters: from colloids to thin films, *Sci. Technol. Adv. Mater.*, 17 (2016) 443–453.
- [20] C. Neaime, M. A. Cortes, F. Grasset, Y. Molard, S. Cordier, B. Dierre, M. Mortier, T. Takei, K. Takahashi, H. Haneda, M. Verelst, S. Lechevallier, Time-gated luminescence bioimaging with new luminescent nanocolloids based on $[\text{Mo}_6\text{I}_8(\text{C}_2\text{F}_5\text{COO})_6]_2$ metal atom clusters, *Phys. Chem. Chem. Phys.*, 18 (2016) 30166-30173.
- [21] T. Aubert, F. C. Hurtado, M. A. Esnault, C. Neaime, D. L. Chauvel, S. Jeanne, P. Pellen, C. Roiland, L. L. Polles, N. Saito, K. Kimoto, H. Haneda, N. Ohashi, F. Grasset, S. Cordier, Extended investigations on luminescent $\text{Cs}_2[\text{Mo}_6\text{Br}_{14}]\text{@SiO}_2$ nanoparticles: physico-structural characterizations and toxicity studies, *J. Phys. Chem. C.*, 117 (2013) 20154–20163.

- [22] F. C. Hurtado, M. D. Lozano-Baena, C. Neaime, A. Burel, S. Jeanne, P. P. Mussi, S. Cordier, F. Grasset, Studies on plant cell toxicity of luminescent silica nanoparticles ($\text{Cs}_2[\text{Mo}_6\text{Br}_{14}]\text{@SiO}_2$) and its constitutive components, *J. Nanopart. Res.*, 18 (2016) 69-84.
- [23] L. M. Rossi, L. Shi, F. H. Quina, Z. Rosenzweig, Stober synthesis of monodispersed luminescent silica nanoparticles for bioanalytical assays, *Langmuir*, 21 (2005) 4277-4280.
- [24] P. A. Bazula, P. M. Arnal, C. Galeano, B. Zibrowius, W. Schmidt, F. Schüth, Highly microporous monodisperse silica spheres synthesized by the Stöber process, *Microporous and Mesoporous Mater.*, 200 (2014) 317-325.
- [25] S. H. Wu, Y. Hung, C.Y. Mou, Compartmentalized hollow silica nanospheres templated from nanoemulsions, *Chem. Mater.*, 25 (2013) 352–364.
- [26] C. T. Yamashita, M. Ando, M. Noritake, H. R. Khosroshahi, M. Fuji, Emulsion templating of poly (acrylic acid) by ammonium hydroxide/sodium hydroxide aqueous mixture for high-dispersed hollow silica nanoparticles, *Advanced Powder Technol.*, 28 (2017) 398-405.
- [27] F. Grasset, F. Dorson, S. Cordier, Y. Molard, C. Perrin, A. M. Marie, T. Sasaki, H. Haneda, Y. Bando, M. Mortier, Water-in-oil microemulsion preparation and characterization of $\text{Cs}_2[\text{M}_6\text{X}_{14}]\text{@SiO}_2$ phosphor nanoparticles based on transition metal clusters (X = Cl, Br, and I), *Adv. Mater.*, 20 (2008) 143-148.
- [28] T. Wang, W. Man, J. Shangguan, W. Jiang, Q. Zhong, Controllable synthesis of hollow mesoporous silica spheres and application as support of nano-gold, *J. Solid State Chem.*, 215 (2014) 67-73.
- [29] Y. S. Lin, S.H. Wu, C.T. Tseng, Y. Hung, C. Chang, C. Y. Mou, Synthesis of hollow

- silica nanospheres with a microemulsion as the template, *Chem. Commun.*, 24 (2009) 3542-3544.
- [30] N. Saito, P. Lemoine, N. Dumait, M. A. Cortes, S. Paofai, T. Roisnel, V. Nassif, F. Grasset, Y. Wada, N. Ohashi and S. Cordier, From $\text{Cs}_2\text{Mo}_6\text{Cl}_{14}$ to $\text{Cs}_2\text{Mo}_6\text{Cl}_{14}\text{H}_2\text{O}$ and vice versa: crystal chemistry investigations, *J. Clust. Sci.*, 28 (2017) 773–798.
- [31] M. Fuji, C. Takai, Y. Tarutani, T. Takei, M. Takahashi, Surface properties of nanosize hollow silica particles on the molecular level, *Advanced Powder Technol.*, 18 (2007) 81-91.
- [32] H. Shi, Y. Wanga, R. Huaa, Acid-catalyzed carboxylic acid esterification and ester hydrolysis mechanism: acylium ion as a sharing active intermediate via a spontaneous trimolecular reaction based on density functional theory calculation and supported by electrospray ionization-mass spectrometry, *Phys. Chem. Chem. Phys.*, 17 (2015) 30279-30291.
- [33] C. S. Cucinotta, A. Ruini , A. Catellani, A. Stirling, Ab initio molecular dynamics study of the keto–enol tautomerism of acetone in solution. *Chem. Phys. Chem.*, 7 (2006) 1229 - 1234.
- [34] T. K. N. Nguyen, B. Dierre, F. Grasset, A. Renaud, S. Cordier, P. Lemoine, N. Ohashi, T. Uchikoshi, Formation mechanism of transparent Mo_6 metal atom cluster film prepared by electrophoretic deposition, *J. The Electrochemical Soc.*, 164 (2017) 412-418.
- [35] Y. A. Vorotnikov, O. A. Efremova, N. A. Vorotnikova, K. A. Brylev, M.V. Edeleva, Al. R. Tsygankova, A. I. Smolentsev, N. Kitamura, Y. V. Mironovad, M.A. Shestopalov, On the synthesis and characterisation of luminescent hybrid particles: Mo_6 metal cluster complex/ SiO_2 , *RSC Adv.*, 6 (2016) 43367-43375.

[36] M. Yang, H.S. Peng, F. Zeng, F. Teng, Z. Qu, D. Yang, Y. Wang, G. Chen, D. Wang, In situ silica coating-directed synthesis of orthorhombic methylammonium lead bromide perovskite quantum dots with high stability, *J. Colloid and Interface Sci.*, 509 (2018) 32-38.

[37] H. Chang Kim, H. G. Hong, C. Yoon, H. Choi, I. S. Ahn, D. C. Lee, Y. J. Kim, K. Lee, Fabrication of high quantum yield quantum dot/polymer films by enhancing dispersion of quantum dots using silica particles, *J. Colloid and Interface Sci.*, 393 (2013) 74-79.

Accepted manuscript